AIAA Propulsion and Energy, July 2018, Cincinnati, OH

An empirical scaling relationship for the total pressure in hollow cathodes

Pierre-Yves C. R. Taunay,*† Christopher J. Wordingham,*

Edgar Y. Choueiri‡

Princeton University, Princeton, NJ, 08544, USA

A non-dimensional scaling relationship for the total pressure inside thermionic, orificed hollow cathodes is derived empirically from a large database of experimental measurements and is analyzed statistically. The relationship allows calculating the total pressure inside hollow cathodes, which is necessary for self-consistent analytical models of the insert region and for insert lifetime calculations. The scaling relationship is a function of cathode operational parameters and is expressed as a non-dimensional power law. It is compared to experimental data for self-consistency and to theoretical modeling efforts. It is found that the empirical correlation agrees with experimental data with an R-squared value of 0.98 and average error of 24.5%, allows calculating the pressure over a range of three orders of magnitude or five orders of magnitude in the non-dimensional space, and is able to capture the dependency of the total pressure on the discharge current where theoretical models can not. For the dataset considered the scaling is shown to be insensitive to variations in the cathode orifice length, propellant ionization energy, and viscosity.

I. Introduction

Successful long-term operation of Hall and ion thrusters depends upon the reliable operation of hollow cathode neutralizers and plasma sources. Requirements for operational power and lifetime for these thrusters continue to increase: "near-term" projected power throughput for next-generation thrusters is expected to be $100 - 200$ kW,[1] with some proposed missions requiring operational lifetimes of up to 100 kh.[2,3] For specific impulses in the range of $2000 - 6000$ s, cathode discharge currents approaching 700 A may be required.[4,5] We have demonstrated operation at up to 400 A in our own work,[6] but without experimental measurements of the emitter temperature profile and internal axial plasma density profile it is challenging to predict the operational lifetime. Widely-applicable and reliable cathode models that do not rely on cathode-specific experimental data as an input are necessary for the development of next-generation hollow cathodes.

In both Refs. 7 and 8, the authors noted that the estimate of the neutral gas pressure in the cathode affects predicted physical quantities such as the electron temperature and the ratio of sheath edge plasma density to the average plasma density. Assuming charge-exchange-dominated ambipolar diffusion, the electron temperature depends only on the geometry of the cathode and the neutral gas density.[8] The neutral gas pressure P_g can then be estimated in both the cathode insert and orifice regions from the total pressure and ionization fraction. The estimation of the latter is beyond the scope of this paper. Calculation of the total pressure has been performed using an empirical relationship designed for a mercury hollow cathode,[9–14] an isentropic[15] or isothermal[16,17] flow approach, Poiseuille flow theory,[18–20] a modification of Poiseuille flow theory[21,22] (to take into account compressibility and molecular flow effects) and an "equivalent temperature" or modified specific gas constant taking into account the ionization fraction.[16,17,23,24]

The empirical approach suggested by Siegfried and Wilbur[9–13] for mercury hollow cathodes and later extended by Friedly to xenon cathodes in Ref. 14 uses relationships based on a single cathode. Similar work by Patterson *et al.*[25] only uses the T6 cathode. The resulting relationships from these approaches cannot

*Graduate Student, MAE Dept., Princeton University, AIAA Student Member.

†Corresponding author: ptaunay@princeton.edu

‡Chief Scientist, EPPDyL, Professor, Applied Physics Group, MAE Dept., Princeton University, AIAA Fellow.

be generalized to other cathodes or operating conditions. Friedly[14] suggests that the mass flow rate used in the empirical relationship be augmented by the ion flow rate ingested by the cathode. The ions are assumed to go through a double-sheath in front of the orifice and recombine in the insert region as neutrals that then exit the orifice. Since Friedly considers that the total flow rate without ion ingestion inside the orifice is that of the supply, the backstreaming ions have to be created through another mechanism outside of the cathode. This approach possibly contradicts conservation of mass.

The isentropic flow model of Ref. 15 relies on the assumptions that the flow is choked at the outlet plane, the flow rate is sufficient to ensure continuum flow in the orifice region, and that both viscous losses and heat addition due to Joule heating are negligible. Similar assumptions are made in Refs. 16 and 17 for an isothermal flow. The choked-flow assumption is justified as long as the ratio of backing (stagnation) pressure P_0 to vacuum background pressure P_b satisfies:

$$\frac{P_0}{P_b} > G = \left(\frac{\gamma+1}{2}\right)^{\gamma/(\gamma-1)}, \tag{1}$$

where γ is the ratio of heat capacities. This condition is met for all cathodes operating in vacuum: for monatomic propellants, $\gamma = 5/3$ and $G = 2.05$. Since most cathodes operate in a vacuum chamber with $P_b \approx 10^{-5}$ Torr or lower or in the vacuum of space, $P_0/P_b \gg G$.

For most cathodes, however, the continuum assumption in the orifice is not guaranteed to hold. Figure 1(a) shows typical values of the Knudsen number, Kn, in the orifice. Knudsen numbers in the range $0.01 < \mathrm{Kn} < 1.0$ indicate the transition regime from continuum to molecular fluid flow. The values are computed using a set of experimental data from Siegfried and Wilbur's mercury cathode,[26] Friedly's cathode,[14] Salhi's xenon and argon cathode,[17] Domonkos's SC012, EK6, and AR3 cathodes,[21] the T6 cathode from the Royal Aerospace Establishment,[25,27] and the NSTAR and NEXIS cathodes from the Jet Propulsion Laboratory.[28–32] The neutral gas temperature is estimated to be either three times the maximum insert wall temperature,[18] or 3000 K if wall temperature data is unavailable. The list of cathodes reviewed is shown in the Appendix.

Viscosity has been underlined as an important process for the flow dynamics inside the cathode in 2D-simulations in Ref. 31. Computed Reynolds numbers Re in Fig. 1(b) indicate that the flow through the cathode can be considered laminar ($\mathrm{Re} \ll 1000$) and that viscous effects are indeed important ($0.1 < \mathrm{Re} < 10$). The dynamic viscosity for the Reynolds number is calculated using results from Stiel and Thodos[33] for xenon and argon. We use the Chapman-Enskog method applied to the Lennard-Jones 12-6 potential for mercury vapor with $\sigma = 2.898\,\text{Å}$ and $\epsilon/k_B = 851.0$ K.[34] This method produces good agreement with experimental data for temperatures less than 1000 K as shown in Fig. 2.

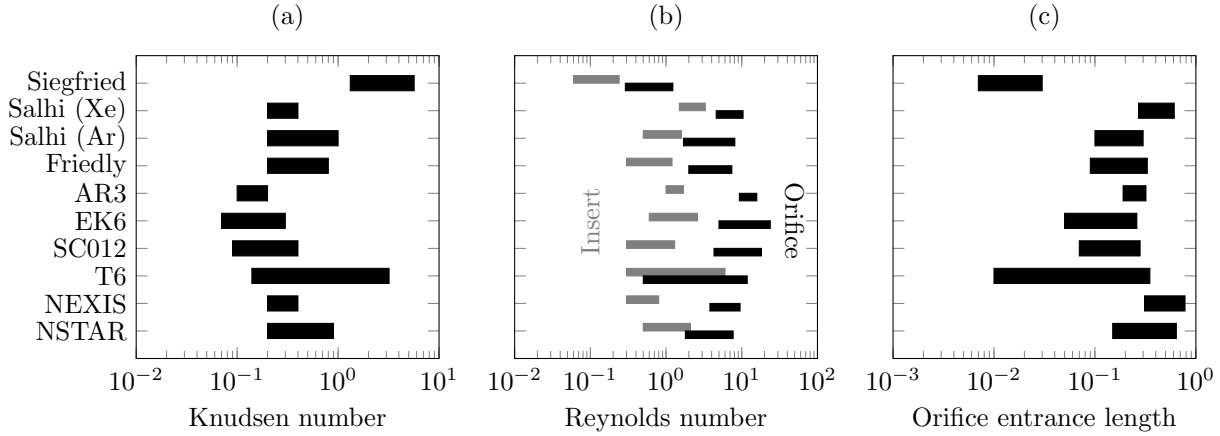

Figure 1: Orifice Knudsen number, range of Reynolds number for both insert and orifice, and orifice entrance length (as a fraction of total orifice length).

Poiseuille flow theory is not applicable in the orifice region. It relies on the assumption of an incompressible, fully-developed, laminar flow, with a no-slip condition at the wall. The latter two are likely applicable in this region, while the former two are not. Poiseuille flow additionally assumes adiabatic flow, which is not

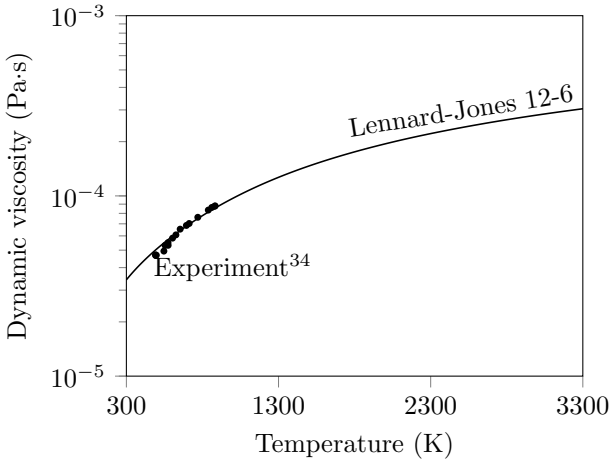

Figure 2: Viscosity of mercury vapor computed with the Chapman-Enskog method applied to a Lennard-Jones 12-6 potential.

valid in most regions of the cathode. Neglecting Joule heating in the flow is problematic because it prevents the model from capturing any effect of the discharge current. The flow transitions from a low Mach number in the insert region to a sonic condition at the orifice outlet and therefore shows strong compressibility effects. The length over which the flow travels before becoming fully-developed or "entrance length" can be estimated with:[35]

$$L_{fd} \approx 0.06 \mathrm{Re} d_o. \tag{2}$$

The range of ratio of L_{fd} to the orifice length L_o is shown in Fig. 1(c) for various cathodes. For most cathodes the effect of the orifice constriction invalidates the fully-developed-flow assumption over the whole length of the orifice. The Poiseuille flow model also does not take into account plasma effects and therefore fails to capture the true dependency of the total pressure with species and discharge current. The latter can change the total pressure significantly, as shown in Fig. 3 where we apply the Poiseuille flow theory to the NEXIS cathode as a function of both discharge current I_d and mass flow rate $\dot{m}$.

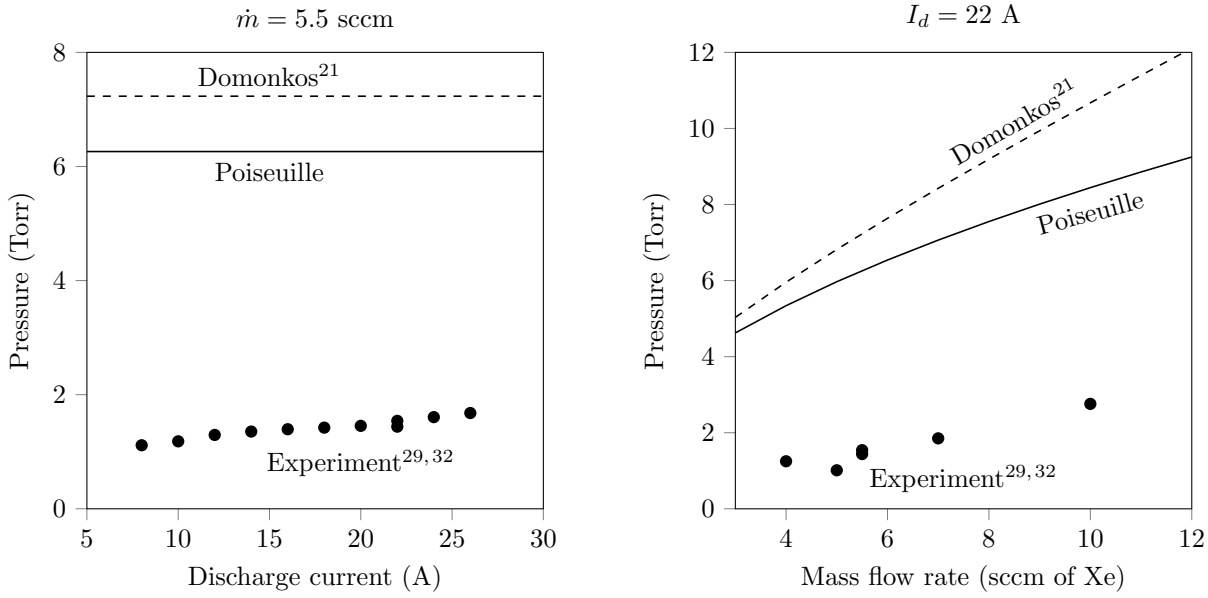

Figure 3: Total pressure for two pressure models as functions of discharge current (left) and mass flow rate (right) for the NEXIS cathode.

More complicated theoretical models such as the one proposed by Domonkos in Refs. 21,22 or Albertoni *et al.* in Refs. 23, 24 attempt to address some of the aforementioned issues. Domonkos suggests combining Poiseuille flow with choked flow condition at the orifice outlet, and adds a correction to the obtained result for the insert-to-orifice constriction and transition to molecular flow. Figure 3 shows that Domonkos's model has worse performance than the Poiseuille approach on the NEXIS cathode, and still cannot capture the effect of the discharge current. Albertoni *et al.*[24] introduce the effect of the plasma through the ionization fraction and electron temperature which are computed as part of a global 0D model. The proposed relationship is used to compute the total static pressure and is valid at the orifice outlet where the author assumes choked flow. This model still relies on Domonkos's modified Poiseuille flow model to predict the pressure drop across the orifice, and therefore cannot accurately account for the effects of Joule heating in the orifice. In addition, the assumptions made in applying Poiseuille flow are generally violated in the cathode orifice as mentioned above.

An analytical description of the flow physics inside the hollow cathode is challenging. The flow features heat addition from Joule heating in the orifice, frozen flow and wall losses due to ionization and plasma sheath fluxes, a transition from incompressible to sonic flow over the length of a short orifice, viscous effects, and a transition to molecular flow. In this work, we propose an empirical approach to calculate the total static pressure inside orificed hollow cathodes and to guide an analytical analysis. We gather experimental data and analyze it using dimensional analysis and propose a power law for the cathode internal pressure as a function of the resulting non-dimensional parameters. We compare the empirical relationship to experimental data and perform a statistical analysis to extract the most pertinent non-dimensional variables. We finally discuss their relevance.

II. Empirical approach

A. Π-products

Based on observation of the experimental data, we expect the cathode pressure to exhibit dependence on geometry, mass flow rate, discharge current, gas species, gas temperature, and viscosity. We therefore consider a general expression for the pressure in the insert region,

$$P = f\left(d_o, d_c, L_o, \dot{m}, I_d, M, a, \epsilon_{iz}, \mu, \mu_0\right), \tag{3}$$

where d_o and d_c are the orifice and insert diameters, respectively, L_o the orifice length, I_d the discharge current, $\dot{m}$ the mass flow rate in kg/s, M the atomic mass of the propellant considered, a the speed of sound of the gas of interest, ϵ_{iz} the ionization energy of the species considered in eV, μ the dynamic viscosity in Pa·s, and μ_0 the permeability of vacuum.

There are four physical dimensions (mass, length, time, charge) and 11 parameters. The Buckingham Π theorem[36] indicates that there should be 7 non-dimensional Π-products. We use Ipsen's method[37] to find the Π-products by successively eliminating physical dimensions from Equation 3. As opposed to the previous empirical studies of Refs. 10 and 14, the total pressure is not normalized by the gasdynamic pressure $P_{\text{gd}} = \dot{m}a/d_o^2$ but by the magnetic pressure $P_{\text{mag}} = \mu_0 I_d^2/d_o^2$. Better agreement to a power law fit is obtained using this approach, especially for cathodes operating at higher discharge currents or lower mass flow rates. We consider the following Π-products:

$$\Pi_1 = \frac{P}{P_{\text{mag}}}, \tag{4}$$

$$\Pi_2 = \frac{d_o}{d_c}, \tag{5}$$

$$\Pi_3 = \frac{d_o}{L_o}, \tag{6}$$

$$\Pi_4 = \left(\frac{\dot{m}q}{MI_d}\right)^2 \left(\frac{Md_o}{\mu_0 q^2}\right), \tag{7}$$

$$\Pi_5 = P_{\mathrm{gd}}/P_{\mathrm{mag}}, \tag{8}$$

$$\Pi_6 = \left(\frac{q\epsilon_{iz}}{\frac{d_o^2 L_o}{P_{\mathrm{mag}}}}\right)\left(\frac{L_o}{d_o}\right), \text{ and} \tag{9}$$

$$\Pi_7 = \mathrm{Re}. \tag{10}$$

We recognize the ratio of total pressure to magnetic pressure in the orifice as the first Π-product. The second and third are geometric aspect ratios. The term $(\dot{m}q/MI_d)$ in the fourth Π-product is the total mass flux divided by the flux of ionized particles and is related to the ionization fraction. The second half of the Π-product is a function of both mass and orifice diameter, and involves both geometry and gas species. The fifth Π-product is the ratio of gasdynamic to magnetic pressures. The numerator of Π_6 is the ionization energy density inside the orifice. It is multiplied by the inverse of Π_3. The seventh Π-product is the Reynolds number and accounts for viscosity effects.

B. Power law

The Π-products are assumed to have a power law dependency:

$$\Pi_1 = C\prod_{k=2}^{7}\Pi_k^{\beta_{k-1}} = \Gamma\left(\Pi\right), \tag{11}$$

where C is a scaling constant, and the β_{k-1} are exponents to be determined. After applying the logarithm base 10 to both sides of Eqn. 11, we obtain a linear relationship:

$$Y = \beta_0 + \sum_{k=2}^{7}\beta_{k-1}X_k, \tag{12}$$

where $Y = \log_{10}\Pi_1$, $X_k = \log_{10}\Pi_k$, and $\beta_0 = \log_{10}C$. Equation 12 is a linear regression which we fit using a least-squares approach.

III. Results and discussion

A. Power law

The least-squares fit yields $\boldsymbol{\beta} = (9.66, 1.43, -0.15, -0.84, 1.89, -0.20, 0.35)$. The corresponding constant for the power law is $C = 4.54 \times 10^9$.

1. Qualitative analysis

The power law fit applied to the experimental data is shown in both Figs. 4(a) and 4(b) for the full data set. The data collapse onto a single line, indicating good agreement with the proposed empirical relationship over a range of five orders of magnitude. Based on the results of the dimensional analysis and the grouping of data by cathode in Fig. 4(b), we can see that as the ratio of the mass flow rate to the discharge current is increased the data points cluster at the origin of the plot. At the opposite end of the curve, data points corresponding to cathodes with relatively high mass flow rate and low discharge current are clustered. Increasing the cathode insert diameter yields results closer to the origin of the plot (e.g. NEXIS cathode), while data points for cathodes with a smaller orifice diameter (e.g. SC012) are clustered towards the high-pressure values. Because the NSTAR, T6, and Salhi's and Siegfried's cathodes have similar dimensions, there is an accumulation of data points at the center of plot.

2. Comparison to theoretical models

The obtained R-squared and average error for the least-squares fit are equal to 0.98 and 24.5%, respectively. The error distribution is shown in Fig. 5 and indicates that the proposed data fit is mostly within a factor of 1.3 of the experimental data. The aforementioned error analysis can be repeated for the isentropic and Poiseuille flow models, as both can be expressed directly in terms of the derived Π-products. The pressure

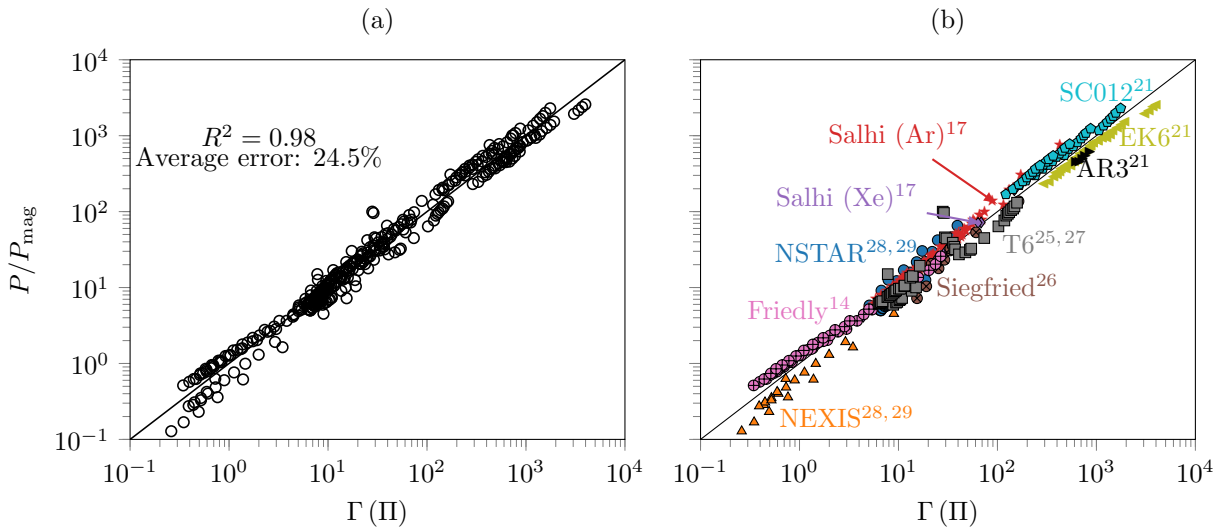

Figure 4: Proposed power law (Eqn. 11) applied to the entire data set.

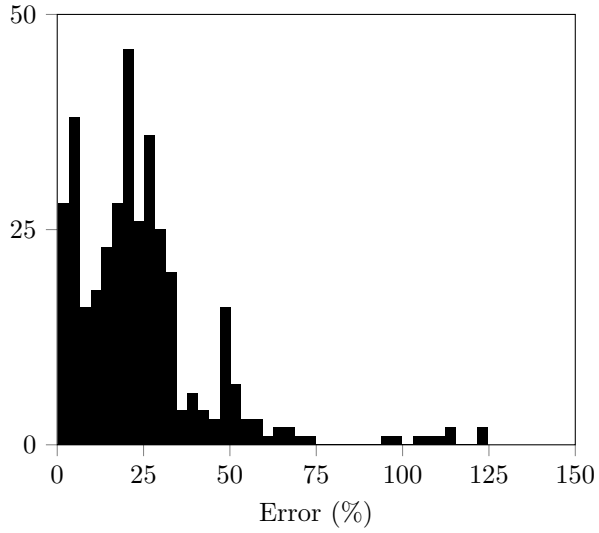

Figure 5: Error histogram for the proposed fit (Eqn. 11).

as calculated from an isentropic flow and Poiseuille flow approach depends only on Π_5, and Π_3, Π_5, and Π_7, respectively:

$$\Pi_1 = C_{\text{iso}}\Pi_5, \tag{13}$$

$$\Pi_1 = C_{\text{Poiseuille}}\Pi_3^{-1/2}\Pi_5\Pi_7^{-1/2}. \tag{14}$$

The constants C_{iso} and $C_{\text{Poiseuille}}$ are the respective scaling constants. Neither approach include a dependency on the plasma quantities and therefore discharge current. The corresponding R-squared value and average errors are shown in Table 1. The high values for the R-squared and average error for both the isentropic and Poiseuille flow models indicate that they are not adequate in capturing the total pressure inside hollow cathodes.

Flow model or empirical relationship	R^2	Average error
Isentropic	0.78	126%
Poiseuille	0.92	84%
Power law	0.98	24.5%

Table 1: R-squared value and average error for the studied flow models and empirical relationship.

3. Statistical analysis

PRINCIPAL COMPONENT ANALYSIS The goal of the principal component analysis (PCA) is to determine the number of relevant variables. PCA calculations are performed with the `scikit-learn` API.[38] Figure 6 shows the explained variance as a function of the total number of variables considered. The variance ceases to increase for three or more dimensions which indicates that the total pressure is not a strong function of three of the Π-products. The redundant Π-products are found by performing two additional analyses.

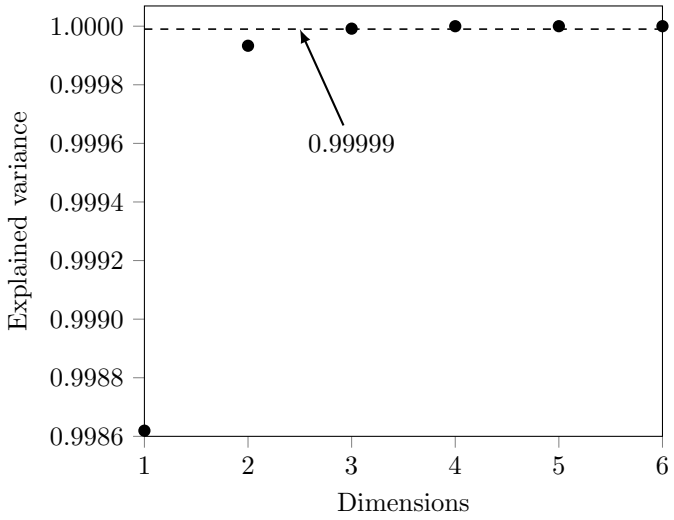

Figure 6: Explained variance for the dataset.

P-VALUES We assess the relevance of each variable by evaluating the following null hypothesis:

$$\text{Null hypothesis 0 (H0): } \beta_k = 0.$$

For all k, we calculate a linear fit without β_k and the corresponding F-statistic:[39]

$$F = \frac{\mathrm{RSS}_k - \mathrm{RSS}}{\dfrac{\mathrm{RSS}}{N-p-1}}, \tag{15}$$

where $N = 366$ is the total size of the dataset, $p = 6$ is the total number of variables, and RSS and RSS_k are the residual sum of squares for the complete and reduced linear fits, respectively:

$$\mathrm{RSS} = \sum_{i=1}^{N} \left(Y_i - \beta_0 - \sum_{k=2}^{7} \beta_{k-1} X_{k,i} \right)^2, \tag{16}$$

$$\mathrm{RSS}_k = \sum_{i=1}^{N} \left(Y_i - \beta_0 - \sum_{\substack{j=2 \\ j \neq k}}^{7} \beta_{j-1} X_{j,i} \right)^2. \tag{17}$$

We then calculate the t-statistic and the p-value for Hyp. H0. The F- and t- statistics and the corresponding p-value are shown in Table 2. The p-value for all Π-products is less than 5%, indicating that Hyp. H0 should be rejected in all cases with 95% confidence. However, both Π_3 and Π_6 feature both a low F-statistic and a high p-value as compared to the other products, which indicates that these two variables may be superfluous. The product with the next lowest F-statistic is Π_7. This suggests that the variable may be redundant as well.

Π-product	F-statistic	t-statistic	p-value
2	1013.	31.8	$< 10^{-6}$
3	5.09	2.26	0.025
4	114.0	10.7	$< 10^{-6}$
5	125.9	11.2	$< 10^{-6}$
6	5.12	2.26	0.024
7	94.4	9.71	$< 10^{-6}$

Table 2: F-statistic, t-statistic, and p-value for each Π-product.

Randomized selection The randomized selection test consists in rearranging the samples of one Π-product at a time at random, performing a linear regression (Eqn. 12), and calculating both the R-squared value and average error. The randomization of a superfluous Π-product has little to no effect on these metric. The corresponding R-squared and average error resulting from this process is shown in Table 3. We observe that both the randomization of Π_3 and Π_6 has little to no effect on the overall fit. This shows that both variables are superfluous as was suggested by the p-value analysis. The process can be repeated once these products are discarded. We find that Π_7 has the lowest effect on the fit during the second iteration and can also be removed from the data fit without introducing large errors.

Perturbed	Iteration 1		Iteration 2	
Π-product	R-squared	Average error (%)	R-squared	Average error (%)
2	0.94	55.3	0.92	67.1
3	0.98	24.9	–	–
4	0.98	26.7	0.89	77.5
5	0.98	27.5	0.45	456.
6	0.98	24.5	–	–
7	0.98	26.4	0.98	30.4
Reference	0.98	24.5	0.98	24.8

Table 3: R-squared value and average error for the linear fit with a randomized Π-product. The data for the unperturbed fit is shown on the Reference line.

Interpretation The three dimensions removed from the original Π-product relationship are Π_3, Π_6, and Π_7. Both L_o and ϵ_{iz} do not show much variation in the dataset: most cathodes studied operate with xenon (identical ionization energy) and feature an orifice length which is always close to 1 mm. The products that feature both quantities (Π_3 and Π_6) have therefore little to no effect on the overall fit. Though viscosity effects are important, 81% of the Reynolds numbers studied are within a single order of magnitude: $1 < \mathrm{Re} < 10$. More variation in the data is needed for these Π-products to be relevant. The variance is explained by the effect of the constriction (Π_2), influence of the plasma (Π_4), and gasdynamic effects (Π_5). Physically, the orifice plate results in a pressure drop. It is therefore unsurprising that Π_2 is of importance. Similarly, both the gasdynamic and plasma effect are relevant in this context and can describe two mechanisms of pressure change due to a change in mass flow rate, current, or both.

The proposed scaling relationship and analysis does not extend to cathodes which operate with a much longer orifice or propellant with a lower ionization energy (e.g. lithium). We also note that the relationship spans five orders of magnitude in variation of the non-dimensional variables, and is not able to capture the

dominant effects of a given flow regime. Finally, it is likely that the true dependency of the pressure does not follow a power law. The latter is a simplification that allows for a rapid analysis and development of a pressure estimate.

B. Predictive capabilities

For a monatomic gas with $\gamma = 5/3$, the empirical relationship can be re-written in terms of physical quantities:

$$P\,(\text{Pa}) = 1.36 \times 10^{-9} \frac{I_d^{0.30} T_g^{0.95} \dot{m}^{0.57} L_o^{0.15}}{M^{0.10} \epsilon_{iz}^{0.20} \mu^{0.35} d_c^{1.43} d_o^{1.71}} \tag{18}$$

$$P\,(\text{Torr}) = 5.08 \times 10^{-8} \frac{I_d^{0.30} T_g^{0.95} \dot{m}_{\text{sccm}}^{0.57} L_{o,\text{cm}}^{0.15} M_a^{0.45}}{\epsilon_{iz}^{0.20} \mu^{0.35} d_{c,\text{cm}}^{1.43} d_{o,\text{cm}}^{1.71}}, \tag{19}$$

where M is the atomic mass of the propellant species in kg and M_a is the atomic mass in amu.

Figure 7 shows the empirical relationship applied to the NEXIS cathode for an assumed gas temperature of $3,000$ K. The empirical relationship is capable of capturing the dependence of the cathode internal pressure on discharge current and yields a good approximation of the total pressure. A sensitivity analysis to the gas temperature is shown in Fig. 8 and reveals that a $\pm 30\%$ change in gas temperature results in a $\pm 25\%$ change in total pressure.

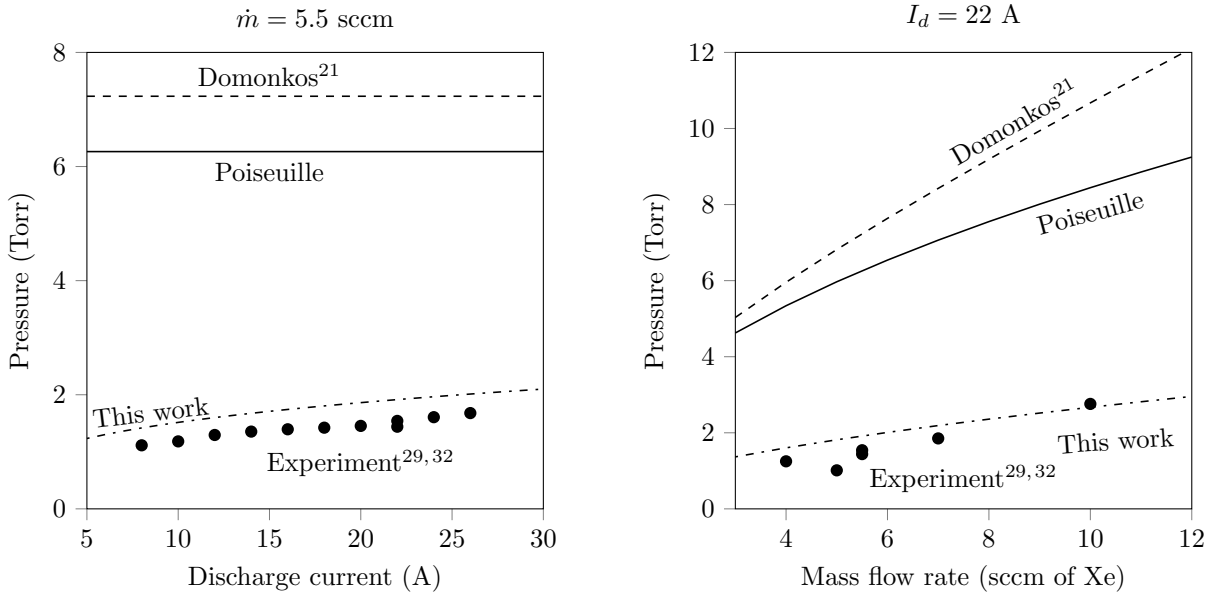

Figure 7: Applied power law to the NEXIS cathode.

IV. Conclusion

We have developed a non-dimensional scaling relationship to calculate the total pressure inside orificed hollow cathodes and compared it to both experimental data for self-consistency and previous modeling attempts. The relationship features good agreement with experimental data and is able to capture the dependency of the pressure with both mass flow rate and discharge current, while theoretical models can not. It is able to capture the pressure over three orders of magnitude or five orders of magnitude in the non-dimensional space. We have used statistical tools to analyze the relationship and found that the influence of the constriction and plasma and gasdynamic effects are the most physically relevant.

Evaluation of the empirical fit based on the derived Π-products allows for the calculation of the cathode internal pressure over an extremely wide range of operating conditions that could not be captured by a flow model incorporating only a single flow regime. This makes the empirical fit a useful tool for the evaluation of future analytical flow models and allows the calculation of previously unknown input values for existing theoretical cathode plasma models.

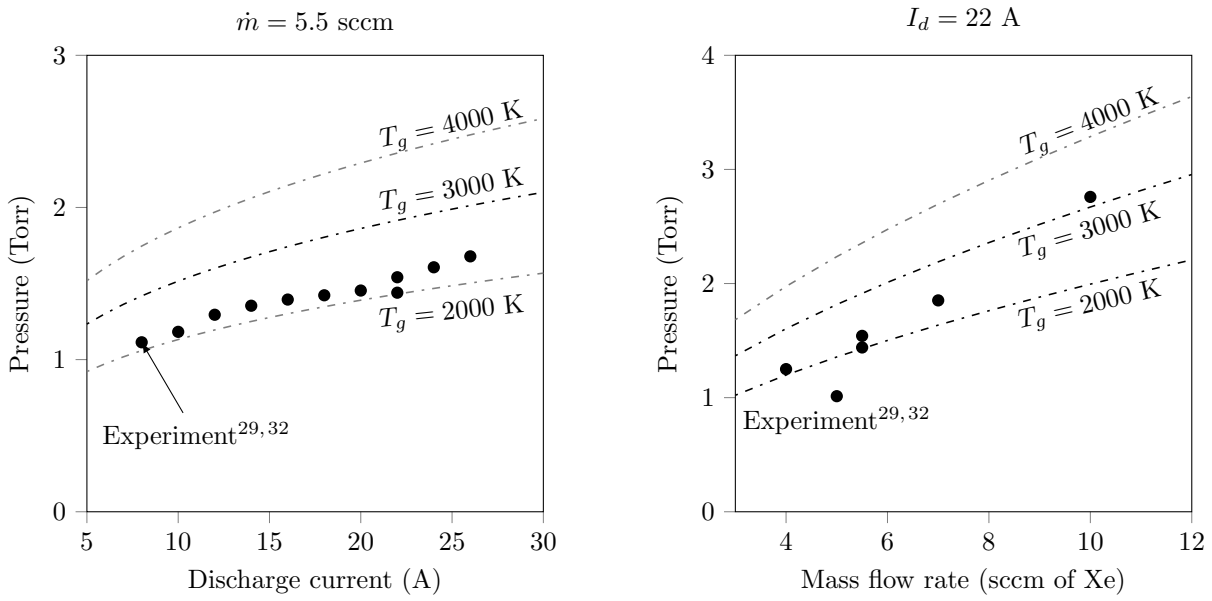

Figure 8: Sensitivity of the proposed empirical law to the gas temperature, applied to the NEXIS cathode.

References

[1]Brown, D. L., et al., "Air Force Research Laboratory High Power Electric Propulsion Technology Development," *IEEE Aerospace Conference*, 2009.

[2]Goebel, D. M. and Chu, E., "High Current Lanthanum Hexaboride Hollow Cathodes for High Power Hall Thrusters," *International Electric Propulsion Conference*, 2011.

[3]Hofer, R.R., et al., "Evaluation of a 4.5 kW Commercial Hall Thruster System for NASA Science Missions," *Joint Propulsion Conference*, 2006.

[4]Plasek, M. L., et al., "Experimental Investigation of a Large-Diameter Cathode," *Joint Propulsion Conference*, 2014.

[5]Goebel, D. M. and Chu, E., "High-Current Lanthanum Hexaboride Hollow Cathode for High-Power Hall Thrusters," *Journal of Propulsion and Power*, 2014.

[6]Wordingham, C. J., et al., "Multiple-Kilowatt-Class Graphite Heater for Large Hollow Cathode Ignition," *Joint Propulsion Conference*, 2015.

[7]Wordingham, C. J., et al., "A Critical Review of Orificed Hollow Cathode Modeling: 0-D Models," *Joint Propulsion Conference*, 2017.

[8]Wordingham, C. J., et al., "Theoretical Prediction of the Dense-Plasma Attachment Length in an Orificed Hollow Cathode," *International Electric Propulsion Conference*, 2017.

[9]Siegfried, D. E. and Wilbur, P. J., "Studies on an experimental quartz tube hollow cathode," *14th International Electric Propulsion Conference*, 1979.

[10]Siegfried, D. E., *A Phenomenological Model for Orificed Hollow Cathodes*, Ph.d., Colorado State University, 1982.

[11]Siegfried, D. E. and Wilbur, P. J., "Phenomenological Model Describing Orificed , Hollow Cathode Operation," *AIAA Journal*, Vol. 21, No. 1, 1983, pp. 5–6.

[12]Siegfried, D. E. and Wilbur, P. J., "A model for mercury orificed hollow cathodes-Theory and experiment," *AIAA journal*, Vol. 22, No. 10, 1984, pp. 1405–1412.

[13]Wilbur, P. J., "Advanced Ion Thruster Research," Tech. Rep. CR-168340, NASA, 1984.

[14]Friedly, V. J., "Hollow Cathode Operation at High Discharge Currents," 1990.

[15]Siegfried, D. and Wilbur, P., "An investigation of mercury hollow cathode phenomena," *13th International Electric Propulsion Conference*, 1978.

[16]Salhi, A. and Turchi, P. J., "Theoretical Modeling of Orificed Hollow Cathode Discharges," *23rd International Electric Propulsion Conference*, 1993.

[17]Salhi, A., *Theoretical and experimental studies of orificed, hollow cathode operation*, Ph.d., The Ohio State University, 1993.

[18]Goebel, D. and Katz, I., *Fundamentals of Electric Propulsion: Ion and Hall Thrusters*, John Wiley & Sons, Inc., 2008.

[19]Mizrahi, J. P., Vekselman, V., Krasik, Y., and Gurovich, V., "0-D Plasma Model for Orificed Hollow Cathodes," *32nd International Electric Propulsion Conference*, 2011.

[20]Mizrahi, J., Vekselman, V., Gurovich, V., and Krasik, Y. E., "Simulation of Plasma Parameters During Hollow Cathodes Operation," *Journal of Propulsion and Power*, Vol. 28, No. 5, 2012, pp. 1134–1137.

[21]Domonkos, M. T., *Evaluation of low-current orificed hollow cathodes*, Ph.d., University of Michigan, 1999.

[22]Domonkos, M. T., "A Particle and Energy Balance Model of the Orificed Hollow Cathode," *38th AIAA/ASME/SAE/ASEE Joint Propulsion Conference & Exhibit*, 2002.

[23]Albertoni, R., *Cathode Processes in MPD Thrusters*, Ph. d., Universita Degli Studi di Pisa, 2012.

[24]Albertoni, R., Pedrini, D., Paganucci, F., and Andrenucci, M., "A Reduced-Order Model for Thermionic Hollow Cathodes," *IEEE Transactions on Plasma Science*, Vol. 41, No. 7, 2013, pp. 1731–1745.

[25]Patterson, S. W. and Fearn, D. G., "The Generation of High Energy Ions in Hollow Cathode Discharges," *26th International Electric Propulsion Conference*, 1999.

[26]Wilbur, P. J., "Ion and Advanced Electric Thruster Research," Tech. Rep. CR-165253, NASA, 1980.

[27]Fearn, D. G. and Patterson, S. W., "Characterisation of the high current hollow cathode for the T6 thruster," *34th AIAA/ASME/SAE/ASEE Joint Propulsion Conference & Exhibit*, 1998.

[28]Jameson, K. K., Goebel, D. M., and Watkins, R. M., "Hollow Cathode and Keeper-Region Plasma Measurements," *41st Joint Propulsion Conference*, 2005.

[29]Jameson, K. K., Goebel, D. M., and Watkins, R. M., "Hollow Cathode and Thruster Discharge Chamber Plasma Measurements Using High-Speed Scanning Probes," *29th International Electric Propulsion Conference*, 2005.

[30]Goebel, D. M. Jameson, K. K. and Katz, I., "Hollow Cathode and Keeper-Region Plasma Measurements Using Ultra-Fast Miniature Scanning Probes," *40th Joint Propulsion Conference*, 2004.

[31]Mikellides, I. G., "Effects of Viscosity in a Partially Ionized Channel Flow with Thermionic Emission," *Physics of Plasmas*, Vol. 16, No. 2005, 2009.

[32]Polk, J., Grubisic, A., Taheri, N., Goebel, D. M., and Hornbeck, S. E., "Emitter Temperature Distributions in the NSTAR Discharge Hollow Cathode," *41st Joint Propulsion Conference*, 2005.

[33]Stiel, L. I. and Thodos, G., "The Viscosity of Nonpolar Gases at Normal," *A.I.Ch.E. Journal*, Vol. 7, No. 4, 1961, pp. 611–615.

[34]Epstein, L. F. and Powers, M. D., "Liquid Metals. I. The Viscosity of Mercury Vapor and the Potential Function for Mercury," *The Journal of Physical Chemistry*, Vol. 57, No. 3, 1953, pp. 336–341.

[35]White, F., *Fluid Mechanics, Sixth Edition*, McGraw-Hill Higher Education, 2008.

[36]Buckingham, E., "On physically similar systems; illustrations of the use of dimensional equations," *Physical Review*, Vol. 4, 1914, pp. 345–376.

[37]Ipsen, E. C., *Units, Dimensions, and Dimensionless Numbers*, McGraw-Hill, 1960.

[38]Pedregosa, F., Varoquaux, G., Gramfort, A., Michel, V., Thirion, B., Grisel, O., Blondel, M., Prettenhofer, P., Weiss, R., Dubourg, V., Vanderplas, J., Passos, A., Cournapeau, D., Brucher, M., Perrot, M., and Duchesnay, E., "Scikit-learn: Machine Learning in Python," *Journal of Machine Learning Research*, Vol. 12, 2011, pp. 2825–2830.

[39]James, G., Witten, D., Hastie, T., and Tibshirani, R., *An Introduction to Statistical Learning*, Springer, 2013.

Appendices

A. List of cathodes

Cathode	Geometry (mm)			P (Torr)	I_d (A)	$\dot{m}$ (eqA)	Species	Refs.
	d_c	d_o	L_o					
Siegfried and Wilbur	3.9	0.76	1.8	1.3 – 6.2	1.27 – 4.3	0.025 – 0.102	Hg	26
Friedly	4.7	0.74	1.0*	5.9 – 53	5.0 – 60	0.18 – 0.46	Xe	14
Salhi	3.81	0.76 – 1.21	1.24	4.8 – 25.2	1.0 – 20.0	0.5 – 1.24	Ar, Xe	17
Domonkos (AR3)	1.22	0.13	0.38	250 – 346	1.0	0.1 – 0.17	Xe	21
Domonkos (EK6)	1.17	0.13	0.71	84 – 598	0.5 – 1.5	0.06 – 0.24		
Domonkos (SC012)	1.8	0.13	0.5	164 – 506	0.5 – 1.5	0.04 – 0.18		
T6	2.0	1.0	2.0	6.4 – 41	5.0 – 15	0.04 – 0.83	Xe	25, 27
NSTAR (discharge)	3.8	1.02	0.74	4.0 – 27.5	6.0 – 15.0	0.18 – 0.72	Xe	28, 31, 32
NEXIS	12.7	1.02	0.74	0.66 – 2.76	4.0 – 32.0	0.298 – 0.72	Xe	29, 30

Table 4: Catalogued cathodes, their operating regime, and the data reference. *The orifice length of the cathode used by Friedly is not specified and set to 1 mm.

B. Π-product exponents

We give the Π-product exponents with additional digits to ensure accurate computations. The pressure

C	$4.542709662295321\times10^{9}$
β_1	1.42823855989297232583
β_2	-0.14530845774509915103
β_3	-0.84243651227508609125
β_4	1.89344785972222107162
β_5	-0.19939669583208508019
β_6	0.34760165492161659850

Table 5: Π-product exponents and constant.

Equations 18 and 19 are given below with additional accuracy:

$$P\,(\text{Pa}) = 1.36115926332423\times10^{-9} I_d^{0.2967706967699} T_g^{0.946723929861111} \dot{m}^{0.556176490093665} L_o^{0.145308457745099} \times \frac{1}{M^{0.104287417586024}\epsilon_{iz}^{0.199396695832085}\mu^{0.347601654921617} d_c^{1.42823855989297} d_o^{1.70771136921674}}. \tag{20}$$

$$P\,(\text{Torr}) = 5.08075608997307\times10^{-8} I_d^{0.2967706967699} T_g^{0.946723929861111} \dot{m}_{\text{sccm}}^{0.556176490093665} L_{o,\text{cm}}^{0.145308457745099} \times \frac{M_a^{0.451889072507641}}{\epsilon_{iz}^{0.199396695832085}\mu^{0.347601654921617} d_{c,\text{cm}}^{1.42823855989297} d_{o,\text{cm}}^{1.70771136921674}}. \tag{21}$$